Differential charge-transfer cross sections for systems with energetically degenerate or near-degenerate channels

H. Nguyen,[1,*] R. Brédy,[1,†] H. A. Camp,[1] T. Awata,[2] and B. D. DePaola[1,‡]
[1]*J. R. Macdonald Laboratory, Department of Physics, Kansas State University, Manhattan, Kansas 66506-2601, USA*
[2]*Department of Physics, Naruto University of Education, Naruto, Tokushima 772-8502, Japan*
(Received 10 December 2003; published 10 September 2004)

Resolution plays a vital role in spectroscopic studies. In the usual recoil-ion momentum spectroscopy (RIMS), *Q*-value resolution is relied upon to distinguish between different collision channels: The better the *Q*-value resolution, the better one is able to resolve energetically similar channels. Although traditional COLTRIMS greatly improves *Q*-value resolution by cooling the target and thus greatly reducing the initial target momentum spread, the resolution of the technique is still limited by target temperature. However, with the recent development in RIMS, namely, magneto-optical trap recoil ion momentum spectroscopy (MOTRIMS) superior recoil ion momentum resolution as well as charge transfer measurements with laser excited targets have become possible. Through MOTRIMS, methods for the measurements of target excited state fraction and kinematically complete relative charge transfer cross sections have been developed, even for some systems having energetically degenerate or nearly degenerate channels. In the present work, the systems of interest having energy degeneracies or near degeneracies are Rb^+, K^+, and Li^+ colliding with trapped Rb(5*l*), where $l=s$ and p.

DOI: 10.1103/PhysRevA.70.032704 PACS number(s): 34.10.+x, 34.20.−b, 34.70.+e, 34.50.Pi

I. INTRODUCTION

In the early 1960s, Everhart and collaborators investigated resonant charge transfer collisions including $He^+ + He$ and $Ne^+ + Ne$ [1]. Measurements of electron transfer probabilities, differential in scattering angle, were made over a wide range of incident energies. However, at that time collisions with excited targets were not examined due to technical difficulties. Near the same time, Perel *et al.* performed a series of experiments investigating total cross sections in symmetric alkali-metal systems [2]. Theoretical and experimental studies for resonant charge transfer cross sections have continued to be investigated. Olson addressed resonant transfer in $Rb^+ + Rb$ theoreticaly [3]. Meanwhile, Bähring and coworkers studied resonant charge transfer in low energy collisions of Na^+ with laser excited $Na^*(3p)$ [4]. Relative differential scattering cross sections for charge transfer were measured over a range of collision energies. Uncertainty in the measurement of target excited state fraction contributed to an overall large uncertainty in the measurement of relative cross sections. Therefore, theoretical comparisons were only made with the measured ground state cross sections. In general, charge transfer cross section measurements from laser-excited targets are made difficult because the transfer rate is proportional to the product of the desired cross section and the relative population of that state. Thus, to obtain the cross section, one must have an independent measurement of the population, and *vice versa*.

Absolute cross sections for single electron transfer of protons and alkali-metal ions have been investigated extensively by Aumayr and coworkers [5]. Dowek and coworkers further studied alkali-metal ions–alkali-metal atoms collision systems [6]. However, simply improving the experimental resolution would not help in the study of degenerate (or nearly degenerate) channels in these systems. How to accurately determine the target excited state fractions was a question which also remained. In this paper we report experimental results obtained from the magneto-optical trap recoil ion momentum spectroscopy (MOTRIMS) apparatus at Kansas State University [7,8]. The setup is a unique probe of target excited state fraction and allows as well the determination of state-selective charge transfer differential cross sections for systems having energetically degenerate or near degenerate channels.

The rest of the paper is organized as follows: The essentials of the MOTRIMS experiment are briefly discussed in Sec. II; the results of the experimental data are given in Sec. III; and a short summary is given in Sec. IV.

II. EXPERIMENT

A complete description of the MOTRIMS apparatus is available elsewhere [7,8]. A simplified schematic of the experimental setup is shown in Fig. 1. Briefly, the apparatus consists of a magneto-optical trap (MOT) [9–11] and a recoil ion momentum spectrometer (RIMS). The MOT consists of a system of diode lasers and accompanying optics, and a pair of anti-Helmholtz coils which are used to set up a magnetic field gradient of approximately 5 G/cm. The target temperature is typically 130 μK, as determined by the "release-and-recapture" method [12,13]. The total target density is ap-

*Present Address: Laboratoire Charles Fabry de l'Institut d'Optique, UMR 8501 du CNRS, 91403 Orsay Cedex, France.
†Present Address: Laboratoire de Spectrométrie Ionique et Moléculaire (LASIM) UMR CNRS 5579 Université Claude Benard Lyon1, 69622 Villeurbanne, France.
‡Corresponding author. Email address: nguyht@phys.ksu.edu/depaola@phys.ksu.edu

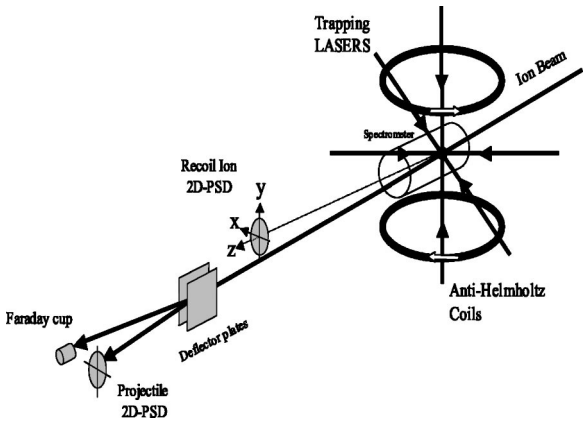

FIG. 1. Simplified schematic diagram of the experimental setup.

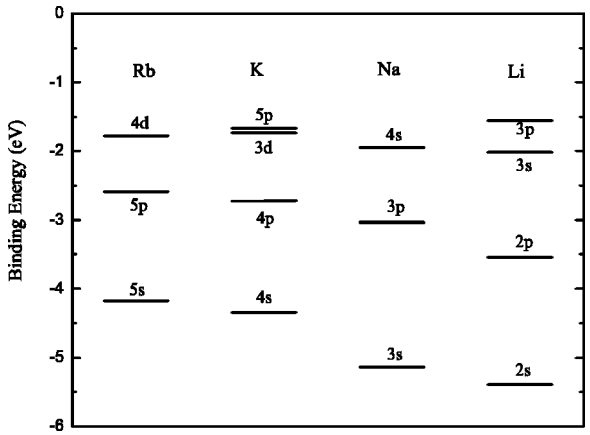

FIG. 2. Energy levels of alkali-metal atoms.

proximately 10^{10} cm^{-3}. The radius of the target is 0.5 mm, and it consists of approximately 10^7 atoms. Background pressure in the collision chamber is typically 4×10^{-9} Torr. The spectrometer consists of a series of metal plates, appropriately biased to create two constant electric field regions, followed by a field-free drift region, followed by a two-dimensional position-sensitive detector (PSD). Singly charged projectile ions created in a thermionic ion source [14] are directed into the target region and from there electrostatically steered into a Faraday cup. If an ion is neutralized through a collision with the Rb target, it passes straight through the electrostatic deflectors and strikes a second PSD. Target ions created in a collision are extracted by the two sequential electric fields, and are allowed to drift in the field-free region before striking the PSD. The spectrometer geometry and electric fields are arranged so as to minimize spread in ion time-of-flight (TOF) and position on the PSD due to initial position. Thus, through the TOF and final position, one may deduce the recoil ion momentum vector at the time of the collision. Because of the combination of the MOT and RIMS techniques, this approach has been dubbed MOTRIMS [15]. A key concept of the RIMS [16–20] method is that one may relate the longitudinal component of the recoil ion momentum to the collision Q-value. For single electron capture

$$Q = -p_{\|}v_p - \frac{m_e}{2}v_p^2, \tag{1}$$

where $p_{\|}$ is the component of recoil momentum parallel to the projectile axis, v_p is the projectile velocity, m_e is the mass of the electron, and Q, the collision Q-value, is defined by

$$Q = E_{\text{initial}}^{\text{binding}} - E_{\text{final}}^{\text{binding}}. \tag{2}$$

The transverse component of the recoil ion momentum $p_{\perp}$, is related to the scattering angle by

$$\theta_p = -\frac{p_{\perp}}{m_p v_p}, \tag{3}$$

where m_p is the projectile mass [17].

The longitudinal momentum component is measured through the difference of the flight times of the projectile and the recoil ion. The perpendicular momentum component is measured through the position of the recoil ion on its position-sensitive detector. In general, the TOF resolution is better than the PSD resolution. Therefore, in order to optimize the resolution in Q-value, the recoil spectrometer used in this work is oriented with its extraction fields nearly parallel to the projectile axis.

III. RESULTS AND DISCUSSION

In this section, we report kinematically complete relative charge transfer cross section measurements from both the ground and first excited states of Rb to the final states of alkali-metal projectiles through energetically degenerate or nearly degenerate channels. The trapping and cooling process leaves some fraction of the Rb in the $5p_{3/2}$ state, and it is critical to determine what is this fraction. As already demonstratd [21,22], target excited state fraction is normally measured by comparing the Q-value spectra taken with the trapping lasers on with those taken with the lasers off. However, inspection of the energy level diagram [23] in Fig. 2, shows that for many systems with energetically similar charge exchange channels, the target excited state fraction is difficult to obtain even with MOTRIMS superior Q-value resolution. Therefore, it has been unclear how to obtain relative capture cross sections for channels that are energetically degenerate or nearly degenerate, e.g., $Rb^+ + Rb(5l) \rightarrow Rb(5l) + Rb^+$, $K^+ + Rb(5l) \rightarrow K(4l) + Rb^+$, and $Li^+ + Rb(5l) \rightarrow Li(2l) + Rb^+$, where $l = s$ and p, since excited state fraction information cannot be accurately measured using the usual Q-value spectra. One might be tempted to look at the target fluorescence to deduce the excited state fraction [24]. However, this method inherently yields excited state fraction results that carry large uncertainty.

A. Side channel method

For the symmetric system 7 keV $Rb^+ + Rb(5l)$, the main capture channels are the resonant ones, i.e., Rb(5s)-Rb(5s) and Rb(5s)-Rb(5s). Because these two channels are resonant, they both have Q-values of zero and hence are indistinguishable in a Q-value spectrum. However, for the projec-

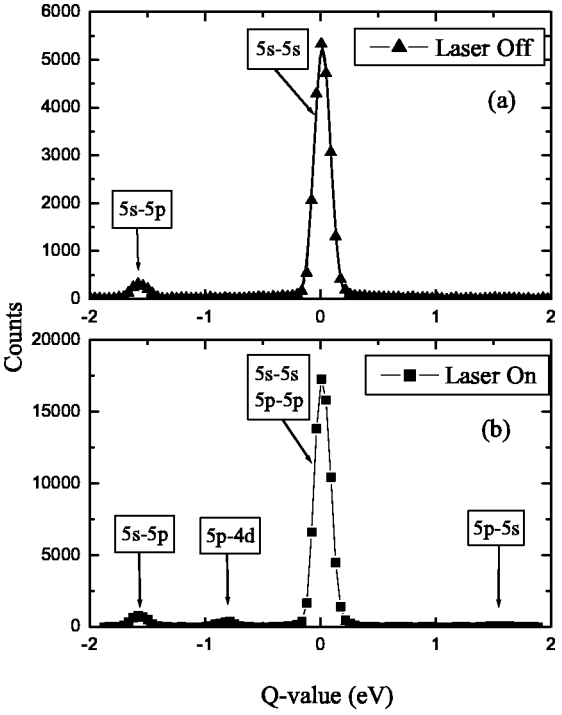

FIG. 3. Counts vs Q-value for 7 keV $Rb^+ + Rb(5l)$, where $l=s$ and p. In (a) the trapping lasers are blocked, while in (b) they are unblocked.

tile energy investigated here, probability for charge transfer through nonresonant channels is large enough to allow a high number of counts through these channels. Using these side peaks along with our proven method [7,21] of chopping trapping the lasers on and off, target excited state fraction was measured. That is, the trapping laser beams were chopped with a 75% on-time duty cycle at 50 kHz. "Laser-on" and "laser-off" Q-value spectra are then compared. Because the atoms do not move an appreciable distance during a single on-off period, the change in Rb(5s) population is exactly equal and opposite to the change in the Rb(5p) population. One can easily show that this allows the determination of both the ratio of the 5s and 5p populations and the ratio of capture cross sections from these states.

As an example, Fig. 3 shows counts *versus* Q-value, for a collision energy of 7 keV. The distinct groups of capture channels are clearly visible. The TOF resolution is between 1 and 2 ns, giving a Q-value resolution for this collision system of 0.18 eV. The limitation to the TOF resolution is believed to be due to the energy spread in the projectile ion beam (1 eV in 7 keV). The TDC (time to digital converter) used to measure the TOF has an inherent resolution limit of 1 ns per channel. Figure 3(a) was taken while the lasers were blocked, while Fig. 3(b) was taken with the lasers unblocked. Thus, the former represents capture from the ground state only, while the latter represents capture from both ground and excited states. In comparing these two plots, the additional channel opened up through capture from Rb(5p) is readily visible. With knowledge of the excited state fraction, these two curves yield relative cross sections for capture, from a pure ground state and a pure excited state, into all of the various final states. The excited state fraction f is measured by observing the change in areas under a single peak representing of capture from the target ground state when the lasers are on and off. In this case, the channel Rb(5s)-Rb(5p) was used to deduce target excited state fraction,

$$f = 1 - \frac{A_{sp}^{\mathrm{on}} T^{\mathrm{off}}}{A_{sp}^{\mathrm{off}} T^{\mathrm{on}}}, \tag{4}$$

where A_{sp}^{on} and A_{sp}^{off} are the number of counts in the channels corresponding to capture from Rb(5s) to Rb(5p) while the lasers are on and off, respectively. T^{on} and T^{off} represent the on and off times for the lasers. The excited state fraction for this particular experiment was found to be 0.23 ± 0.02. From excited state fraction information, contributions to the zero Q-value peak from Rb(5s) to Rb(5s) (A_{ss}^{on}) and Rb(5p) to Rb(5p) (A_{pp}^{on}) channels are given by

$$A_{ss}^{\mathrm{on}} = A_{ss}^{\mathrm{off}} \frac{T^{\mathrm{on}}}{T^{\mathrm{off}}} (1 - f) \tag{5}$$

and

$$A_{ss,pp}^{\mathrm{on}} = A_{ss}^{\mathrm{on}} + A_{pp}^{\mathrm{on}}, \tag{6}$$

where $A_{ss,pp}^{\mathrm{on}}$ is the total number of counts in the resonant channels while the lasers are on.

Furthermore, by knowing the target excited state fraction, one can deduce the kinematically complete relative cross sections from the Q-value spectrum. That is,

$$\frac{\sigma_p}{\sigma_s} = \frac{1 - f}{f} \frac{\sum A_p}{\sum A_s}, \tag{7}$$

where f is the measured excited state fraction of Rb target. ΣA_p and ΣA_s represent the combined areas under all the Q-value peaks for all channels capture from Rb(5p) and Rb(5s), respectively. Experimental results are shown in Table I.

By subtracting laser-off scattering angle data from the laser-on scattering angle data, one obtains the differential cross sections for the completely degenerate channels, namely, capture from Rb(5s) to Rb(5s) and capture from Rb(5p) to Rb(5p) were also measured and are shown in Fig. 4. The oscillatory structure seen in the Rb(5s) to Rb(5s) channel is due to interference between Σ_u and Σ_g in the ground state molecular potential of Rb_2^+ system. The structure is washed out for the case of Rb(5p) to Rb(5p) because of the many interferences from the $\Sigma_{g,u}$ and $\Pi_{g,u}$.

B. Dual beam method

For some systems, e.g, $Li^+ + Rb(5l)$, and $K^+ + Rb(5l)$ excited state fractions cannot be measured from Q-value spectra because for these systems, no pure single peak corresponding to capture from ground state Rb(5s) exists. In this case, an ion source producing two different types of projectiles simultaneously, one of which is Na^+ was used. Because the two ion species have the same energy, but different masses, the capture channels for the different projectile spe-

TABLE I. Experimental relative charge transfer cross sections for 7 keV $Rb^+ + Rb(5l)$, where $l = s$ and p.

Channels	Relative cross sections
$\frac{\sigma_{5p-5p}}{\sigma_{5p}}$	0.89±0.10
$\frac{\sigma_{5p-4d}}{\sigma_{5p}}$	0.09±0.01
$\frac{\sigma_{5p-5s}}{\sigma_{5p}}$	0.02±0.01
$\frac{\sigma_{5s-5s}}{\sigma_{5s}}$	0.94±0.11
$\frac{\sigma_{5s-5p}}{\sigma_{5s}}$	0.06±0.01
$\frac{\sigma_{5p}}{\sigma_{5s}}$	0.95±0.13

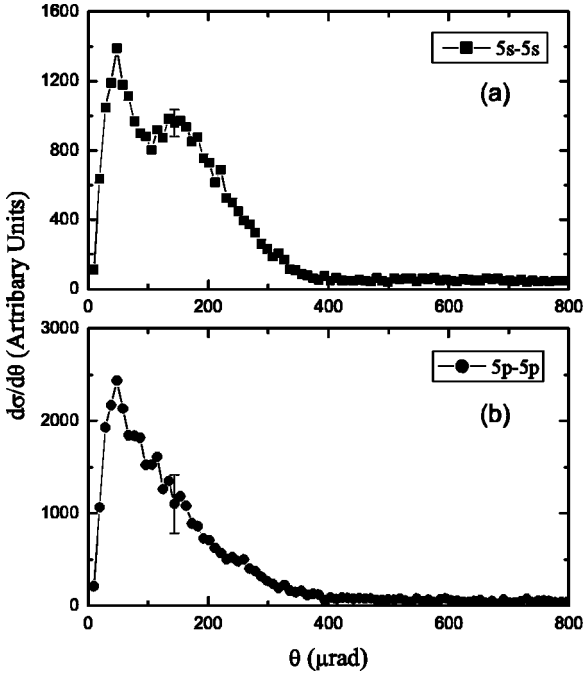

FIG. 4. Differential resonant charge transfer cross sections for 7 keV Rb(5*s*)-Rb(5*s*) in (a) and Rb(5*p*)-Rb(5*p*) in (b).

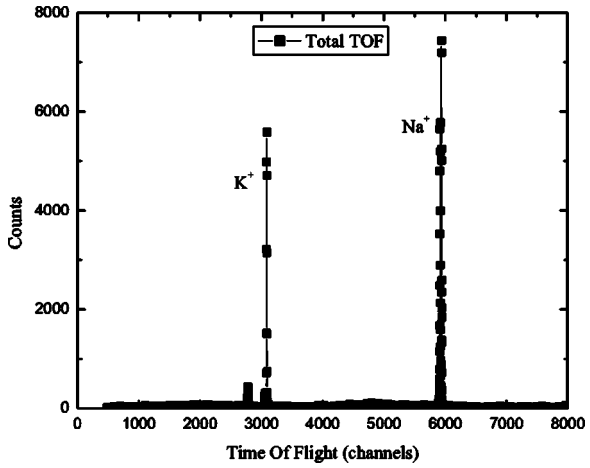

FIG. 5. Total time of flight observed for dual beams method. Recoil ion signatures from collision with both Na^+ and K^+ projectiles can be seen.

cies are well-separated in the time of flight or *Q*-value spectra. In this way, the Na^+ ions can be used to obtain the excited state fraction, while the capture cross sections are measured for the other projectile species.

1. 7 keV $K^+ + Rb(5l)$

Here, the dual beam method is employed to investigate the 7 keV $K^+ + Rb(5l)$ system. Figure 5 shows a complete time of flight spectrum which includes recoil ion signatures for coincidences from both the Na^+ and K^+ projectiles. By "zooming in" on the Na^+ portion of the spectrum, one can measure the excited state fraction of the Rb target. Figure 6 shows coincidences with the Na^+ projectile. The upper and lower panels show the *Q*-value spectra when then lasers are on and off, respectively. The target excited state fraction is obtained from [similar to Eq. (4)]

$$f = 1 - \frac{A_{ss}^{\mathrm{on}} T^{\mathrm{off}}}{A_{ss}^{\mathrm{off}} T^{\mathrm{on}}}, \tag{8}$$

where A_{ss}^{on} and A_{ss}^{off} are counts from the Rb(5*s*) to Na(3*s*) capture channel when the lasers are on and off, respectively. For this particular experiment the excited state fraction was 0.21±0.02. Knowing the target excited state fraction, one can deduce the kinematically complete relative cross sections for the system 7 keV $K^+ + Rb(5l)$ from the *Q*-value spectrum of Fig. 7, using Eq. (7).

In order to differentiate between overlapping channels in ΣA_p and ΣA_s we again use the excited state fraction information [similar to Eq. (5)]

$$A_{nl-n'l'}^{\mathrm{on}} = A_{nl-n'l'}^{\mathrm{off}} \frac{T^{\mathrm{on}}}{T^{\mathrm{off}}} (1 - f), \tag{9}$$

where nl and n$'l'$ are initial and final states, respectively. The experimental relative cross section results for this system are presented in Table II. Scattering angle results for the main charge exchange channels were also obtained and are shown in Fig. 8.

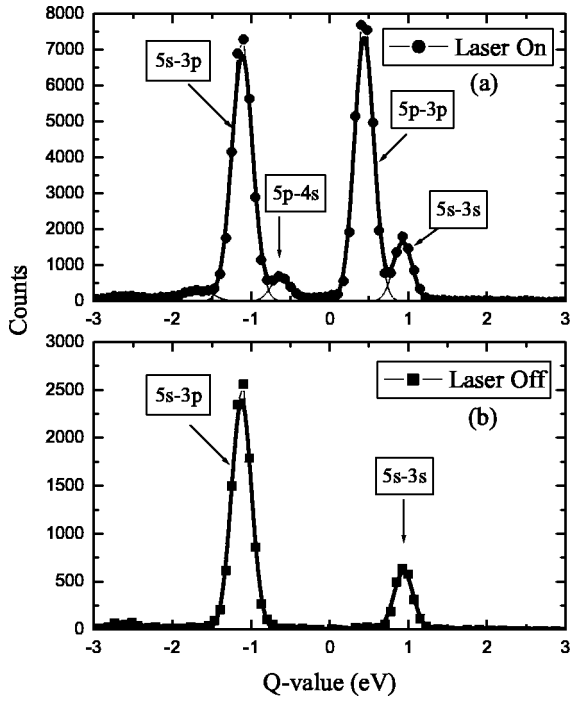

FIG. 6. *Q*-value spectrum of $Na^+ + Rb(5l)$, where $l=s$ and p, system in the Na^+ and K^+ dual beam TOF. The upper panel (a) is the *Q*-value spectrum when lasers are on while the lower panel (b) is the *Q*-value spectrum when lasers are off.

2. 7 keV $Li^+ + Rb(5l)$

The dual beam method is again used to measure relative cross sections for the 7 keV $Li^+ + Rb(5l)$ system. Here, because the Na^+ component of our dual beam source was so weak, the $Na^+ + Rb$ collision system used to deduce excited state fraction yielded inadequate counts in the Rb(5*s*)-Na(3*p*) channel as can be seen in Fig. 9. This would have yielded large error bars in the excited state fraction determination. However, from first principles,

$$A_s^{\text{off}} \propto \sigma_s (n_s^{\text{on}} + n_p^{\text{on}}) T^{\text{off}}, \tag{10}$$

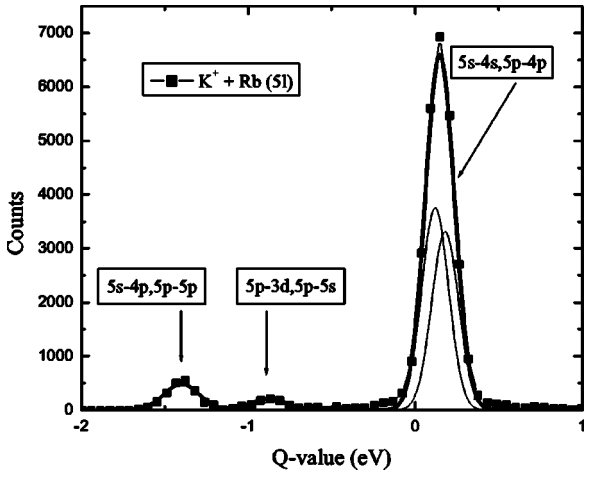

FIG. 7. *Q*-value spectrum of $K^+ + Rb(5l)$, where $l=s$ and p.

TABLE II. Experimental relative charge transfer cross sections for 7 keV $K^+ + Rb(5l)$, where $l=s$ and p.

Channels	Relative cross sections
$\frac{\sigma_{5p-5p}}{\sigma_{5p}}$	0.00±0.03
$\frac{\sigma_{5p-4p}}{\sigma_{5p}}$	0.85±0.18
$\frac{\sigma_{5p-3d}+\sigma_{5p-5s}}{\sigma_{5p}}$	0.15±0.04
$\frac{\sigma_{5s-4s}}{\sigma_{5s}}$	0.91±0.04
$\frac{\sigma_{5s-4p}}{\sigma_{5s}}$	0.09±0.01
$\frac{\sigma_{5p}}{\sigma_{5s}}$	1.4±0.3

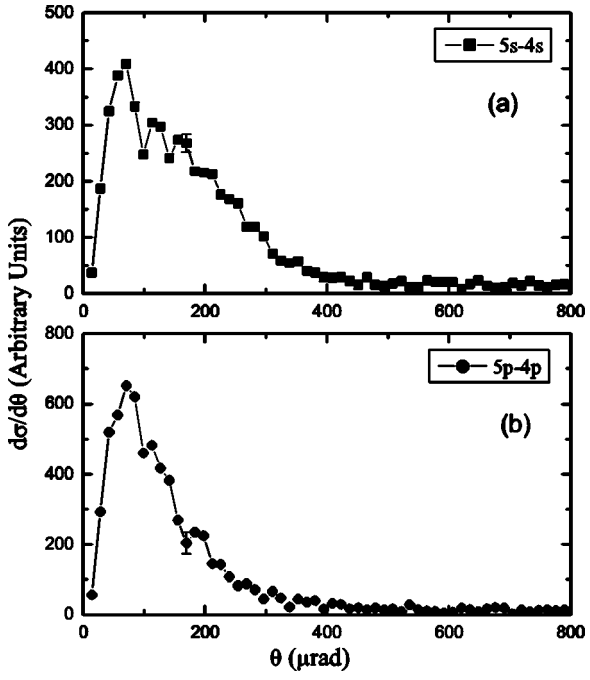

FIG. 8. Differential charge transfer cross sections for 7 keV Rb(5*s*)-K(4*s*) in (a) and Rb(5*p*)-K(4*p*) in (b).

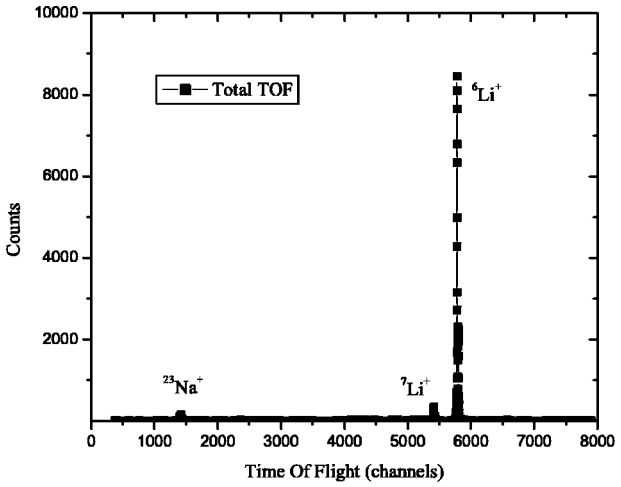

FIG. 9. Total time of flight observed for dual beams method. Recoil ion signatures from collision with both Na^+ and Li^+ projectiles can be seen.

$$A_s^{\mathrm{on}} \propto \sigma_s n_s^{\mathrm{on}} T^{\mathrm{on}}, \tag{11}$$

$$A_p^{\mathrm{on}} \propto \sigma_p n_p^{\mathrm{on}} T^{\mathrm{on}}, \tag{12}$$

where A_s^{on} and A_s^{off} are total capture areas from Rb(5*s*) when the lasers are on and off, respectively. A_p^{on} is the total capture from Rb(5*p*) when the lasers are on. From the equations above, the target excited fraction, *f*, can be obtained via

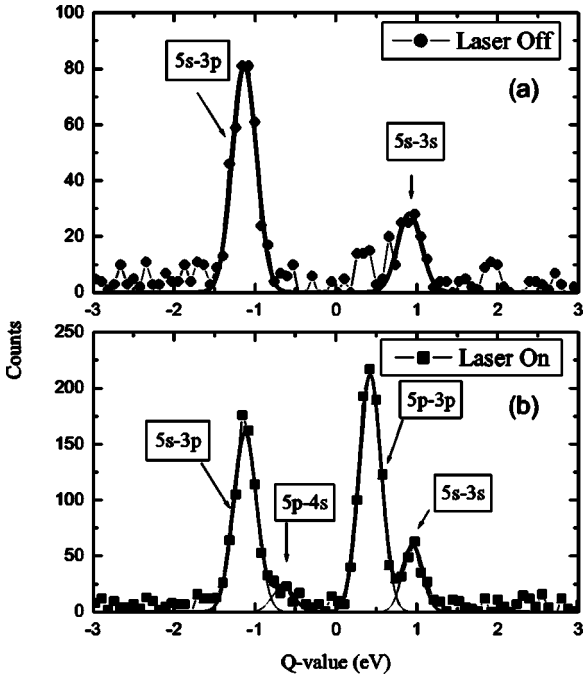

FIG. 10. *Q*-value spectrum of $Na^+ + Rb(5l)$, where $l=s$ and p, system in the Na^+ and Li^+ dual beam TOF. The upper panel (a) is the *Q*-value spectrum when lasers are off while the lower panel (b) is the *Q*-value spectrum when lasers are on.

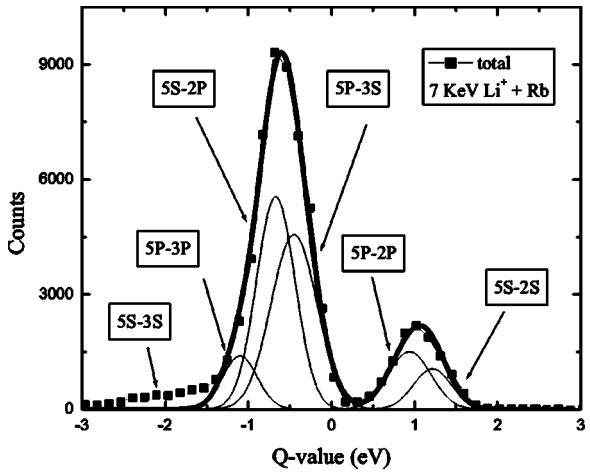

FIG. 11. *Q*-value spectrum of $Li^+ + Rb(5l)$, where $l=s$ and p.

$$f = \frac{A_p^{\mathrm{on}} T^{\mathrm{off}} \sigma_s}{A_s^{\mathrm{off}} T^{\mathrm{on}} \sigma_p}. \tag{13}$$

The ratio σ_p/σ_s for 7 keV $Na^+ + Rb(5l)$, where $l=s$ and p, is known with high accuracy through the completely independent experiments and were shown to be in good agreement with theoretical prediction [22] (see Fig. 10). The ratio $A_p^{\mathrm{on}}/A_s^{\mathrm{off}}$ was measured from the Q-value spectrum gated on

TABLE III. Experimental relative charge transfer cross sections for 7 keV $Li^+ + Rb(5l)$, where $l=s$ and p.

Channels	Relative cross sections
$\frac{\sigma_{5p-3p}}{\sigma_{5p}}$	0.33±0.04
$\frac{\sigma_{5p-3s}}{\sigma_{5p}}$	0.47±0.06
$\frac{\sigma_{5p-2p}}{\sigma_{5p}}$	0.20±0.03
$\frac{\sigma_{5s-2s}}{\sigma_{5s}}$	0.17±0.08
$\frac{\sigma_{5s-2p}}{\sigma_{5s}}$	0.83±0.02
$\frac{\sigma_{5p}}{\sigma_{5s}}$	0.67±0.09

the $Na^+ + Rb(5l)$ collisions as in Fig. 10. For this particular experiment, the target excited state fraction was measured to be 0.19 ± 0.04.

From Eqs. (10) and (12),

$$\frac{\sigma_p}{\sigma_s} = \frac{A_p^{\text{on}} T^{\text{off}}}{A_s^{\text{off}} T^{\text{on}} f}. \tag{14}$$

Here, A_s^{off} and A_p^{on} are total areas in capture from Rb(5*s*) when the lasers are off, and total areas in capture from Rb(5*p*) when the lasers are on for the $Li^+ + Rb(5l)$ collision system. These areas can be extracted from Fig. 11. In order to differentiate between overlapping channels, as seen in Fig. 11, we again used the excited state fraction information through the formalism presented in Eq. (9).

The experimental relative cross section results for this system are presented in Table III. The charge transfer channel Rb(5*s*)-Li(2*p*) dominates the total capture from Rb(5*s*). Charge transfer from Rb(5*p*) is more uniformly distributed among the three major channels. Differential cross sections in term of scattering angles are also measured. Shown in Fig. 12 are the differential cross sections for the two dominant capture channels Rb(5*p*)-Li(2*p*) and Rb(5*s*)-Li(2*s*). In both of these, a hint of structure can be seen just beyond the present resolving power of the apparatus.

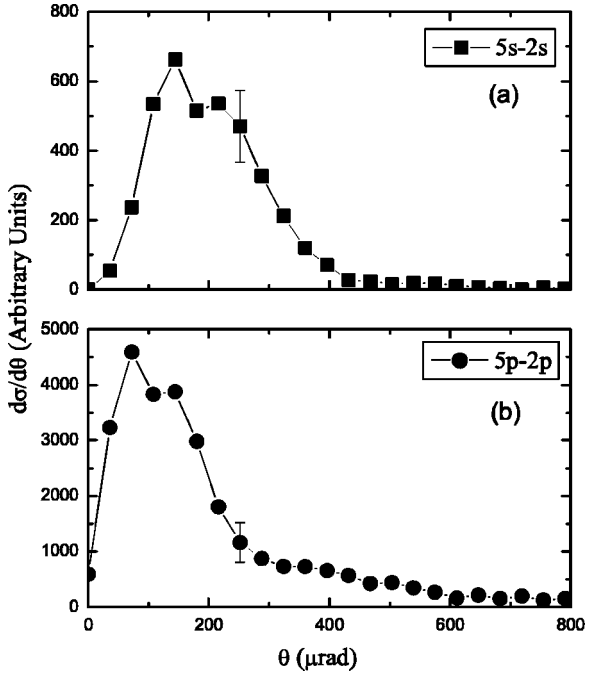

FIG. 12. Differential charge transfer cross sections for 7 keV Rb(5*s*)-Li(2*s*) in (a) and Rb(5*p*)-Li(2*p*) in (b).

IV. SUMMARY

In summary, kinematically complete relative cross section measurements for resonant and near resonant charge transfer channels from a target in a mixture of ground and excited states were made. A combination of two projectile species was used to make detailed measurements of relative charge transfer cross sections for $Li^+ + Rb(5l)$ and $K^+ + Rb(5l)$ collisions at impact energies of 7 keV. Cross sections differential in scattering angle were also obtained for the dominant charge transfer channels in these system. For the symmetric system Rb^+-Rb(5*l*), the dual beam method was not necessary for the identification and separation of energetically degenerate channels. However, the dual beam method of obtaining target excited state fractions will work well for Rb^+-Rb at lower energies where capture from Rb(5*s*) to Rb(5*p*) is small, making the overall count rate for this channel insufficient for excited state fractions measurement.

ACKNOWLEDGMENT

This work was supported by the Chemical Sciences, Geosciences and Biosciences Division, Office of Basic Energy Sciences, Office of Science, U. S. Department of Energy.

[1] G. J. Lockwood, H. F. Helbig, and E. Everhart, Phys. Rev. **132**, 2078 (1963).
[2] J. Perel, R. H. Vernon, and H. L. Daley, Phys. Rev. **138**, A937 (1965).
[3] R. E. Olson, Phys. Rev. **187**, 153 (1969).
[4] A. Bähring, I. V. Hertel, E. Meyer, and H. Schmidt, Phys. Rev. Lett. **53**, 1433 (1984).
[5] F. Aumayr, G. Lakits, and H. Winter, J. Phys. B **20**, 2025 (1987), and references therein.
[6] D. Dowek *et al.*, J. Phys. B **35**, 2051 (2002), and references therein.
[7] H. Nguyen, X. Fléchard, R. Brédy, H. A. Camp, and B. D. DePaola, Rev. Sci. Instrum. **75**, 2638 (2004).
[8] H. Nguyen, Ph.D. thesis, J. R. Macdonald, Laboratory, Kansas State University, Kansas. 2003.
[9] E. L. Raab, M. Prentiss, A. Cable, S. Chu, and D. E. Pritchard, Phys. Rev. Lett. **59**, 2631 (1987).
[10] C. Wieman, G. Flowers, and S. Gilbert, Am. J. Phys. **63**, 4 (1995).
[11] H. Metcalf and P. van der Straten, *Cooling and Trapping of Neutral Atoms* (Springer, New York, 1999).
[12] I. Yavin, M. Weel, A. Andreyuk, and A. Kumarakrishnan, Am. J. Phys. **70**, 2 (2002).
[13] D. S. Weiss, E. Riis, Y. Shevy, P. J. Ungar, and S. Chu, J. Opt. Soc. Am. B **6**, 2072 (1989).
[14] Phrasor Scientific, 1536 Highland Ave, Duarte, CA 91010, USA.
[15] X. Fléchard, H. Nguyen, E. Wells, I. Ben-Itzhak, and B. D. DePaola, Phys. Rev. Lett. **87**, 123203 (2001).
[16] J. Ullrich, R. Moshammer, O. Jagutzki, V. Mergel, H. Schmidt-Böcking, and L. Spielberger, J. Phys. B **30**, 2917 (1997).
[17] R. Dörner, V. Mergel, O. Jagutzki, L. Spielberger, J. Ullrich, R. Moshammer, and H. Schmidt-Böcking, Phys. Rep. **330**, 95

(2000).
[18] R. Moshammer, M. Unverzagt, W. Schmitt, J. Ullrich, and H. Schmidt-Böcking, Nucl. Instrum. Methods Phys. Res. B **108**, 425 (1996).
[19] H. Kollmus, W. Schmitt, R. Moshammer, M. Unverzagt, and J. Ullrich, Nucl. Instrum. Methods Phys. Res. B **124**, 377 (1997).
[20] J. Ullrich, R. Moshammer, A. Dorn, R. Dörner, L. Ph. H. Schmidt, and H. Schmidt-Böcking, Rep. Prog. Phys. **66**, 1463 (2003).
[21] X. Fléchard, H. Nguyen, R. Brédy, S. R. Lundeen, M. Stauffer, H. A. Camp, C. W. Fehrenbach, and B. D. DePaola, Phys. Rev. Lett. **91**, 243005 (2003).
[22] T. G. Lee, H. Nguyen, X. Fléchard, B. D. DePaola, and C. D. Lin, Phys. Rev. A **66**, 042701 (2002).
[23] C. E. Moore, *Atomic Energy Levels* (National Bureau of Standards, Washington, D.C., 1971), Vols. I and II.
[24] C. G. Townsend *et al.*, Phys. Rev. A **52**, 1423 (1995).